ACS SENSORS

Article

Cite This: ACS Sens. 2019, 4, 379−388

pubs.acs.org/acssensors

Soft, Skin-Integrated Multifunctional Microfluidic Systems for Accurate Colorimetric Analysis of Sweat Biomarkers and Temperature

Jungil Choi,[†,‡] Amay J. Bandodkar,[†,‡] Jonathan T. Reeder,[†,‡] Tyler R. Ray,[†,‡] Amelia Turnquist,[§] Sung Bong Kim,[∥] Nathaniel Nyberg,[⊥] Aurélie Hourlier-Fargette,[†,‡] Jeffrey B. Model,[‡,#] Alexander J. Aranyosi,[‡,#] Shuai Xu,[▽] Roozbeh Ghaffari,[‡,#,○] and John A. Rogers*[,†,‡,∥,#,○,◆,¶,+]

[†]Department of Materials Science and Engineering, Northwestern University, Evanston, Illinois 60208, United States

[‡]Center for Bio-Integrated Electronics, Simpson Querrey Institute for BioNanotechnology, Northwestern University, Evanston, Illinois 60208, United States

[§]Department of Chemical Engineering, Northwestern University, Evanston, Illinois 60208, United States

[∥]Department of Materials Science and Engineering, and Frederick Seitz Materials Research Laboratory, University of Illinois at Urbana−Champaign, Urbana, Illinois 61801, United States

[⊥]Department of Mechanical Engineering, Northwestern University, Evanston, Illinois 60208, United States

[#]Epicore Biosystems, Inc., Cambridge, Massachusetts, 02139, United States

[▽]Department of Dermatology, Feinberg School of Medicine, Northwestern University, Chicago, Illinois 60611, United States

[○]Department of Chemistry and Biomedical Engineering, Northwestern University, Evanston, Illinois 60208, United States

[◆]Department of Electrical Engineering and Computer Science, Northwestern University, Evanston, Illinois 60208, United States

[¶]Department of Neurological Surgery, Northwestern University, Evanston, Illinois 60208, United States

[+]Department of Chemistry, Northwestern University, Evanston, Illinois 60208, United States

Supporting Information

ABSTRACT: Real-time measurements of the total loss of sweat, the rate of sweating, the temperature of sweat, and the concentrations of electrolytes and metabolites in sweat can provide important insights into human physiology. Conventional methods use manual collection processes (e.g., absorbent pads) to determine sweat loss and lab-based instrumentation to analyze its chemical composition. Although such schemes can yield accurate data, they cannot be used outside of laboratories or clinics. Recently reported wearable electrochemical devices for sweat sensing bypass these limitations, but they typically involve on-board electronics, electrodes, and/or batteries for measurement, signal processing, and wireless transmission, without direct means for measuring sweat loss or capturing and storing small volumes of sweat. Alternative approaches exploit soft, skin-integrated microfluidic systems for collection and colorimetric chemical techniques for analysis. Here, we present the most advanced platforms of this type, in which optimized chemistries, microfluidic designs, and device layouts enable accurate assessments not only of total loss of sweat and sweat rate but also of quantitatively accurate values of the pH and temperature of sweat, and of the concentrations of chloride, glucose, and lactate across physiologically relevant ranges. Color calibration markings integrated into a graphics overlayer allow precise readout by digital image analysis, applicable in various lighting conditions. Field studies conducted on healthy volunteers demonstrate the full capabilities in measuring sweat loss/rate and analyzing multiple sweat biomarkers and temperature, with performance that quantitatively matches that of conventional lab-based measurement systems.

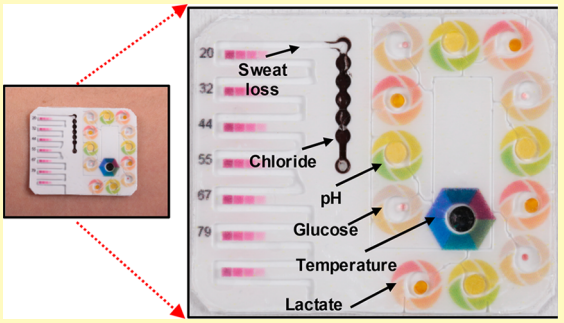

KEYWORDS: *sweat, epidermal, colorimetric, microfluidics, capillary bursting valve*

Eccrine sweat contains a rich mixture of metabolites, proteins, hormones, and electrolytes that reflect physiological conditions and provide information on hydration level. Changes in the concentration of these biomarkers and the rate of sweat excretion correlate to disease states (e.g., cystic fibrosis,

Received: October 11, 2018
Accepted: January 16, 2019
Published: February 1, 2019

DOI: 10.1021/acssensors.8b01218
ACS Sens. 2019, 4, 379−388

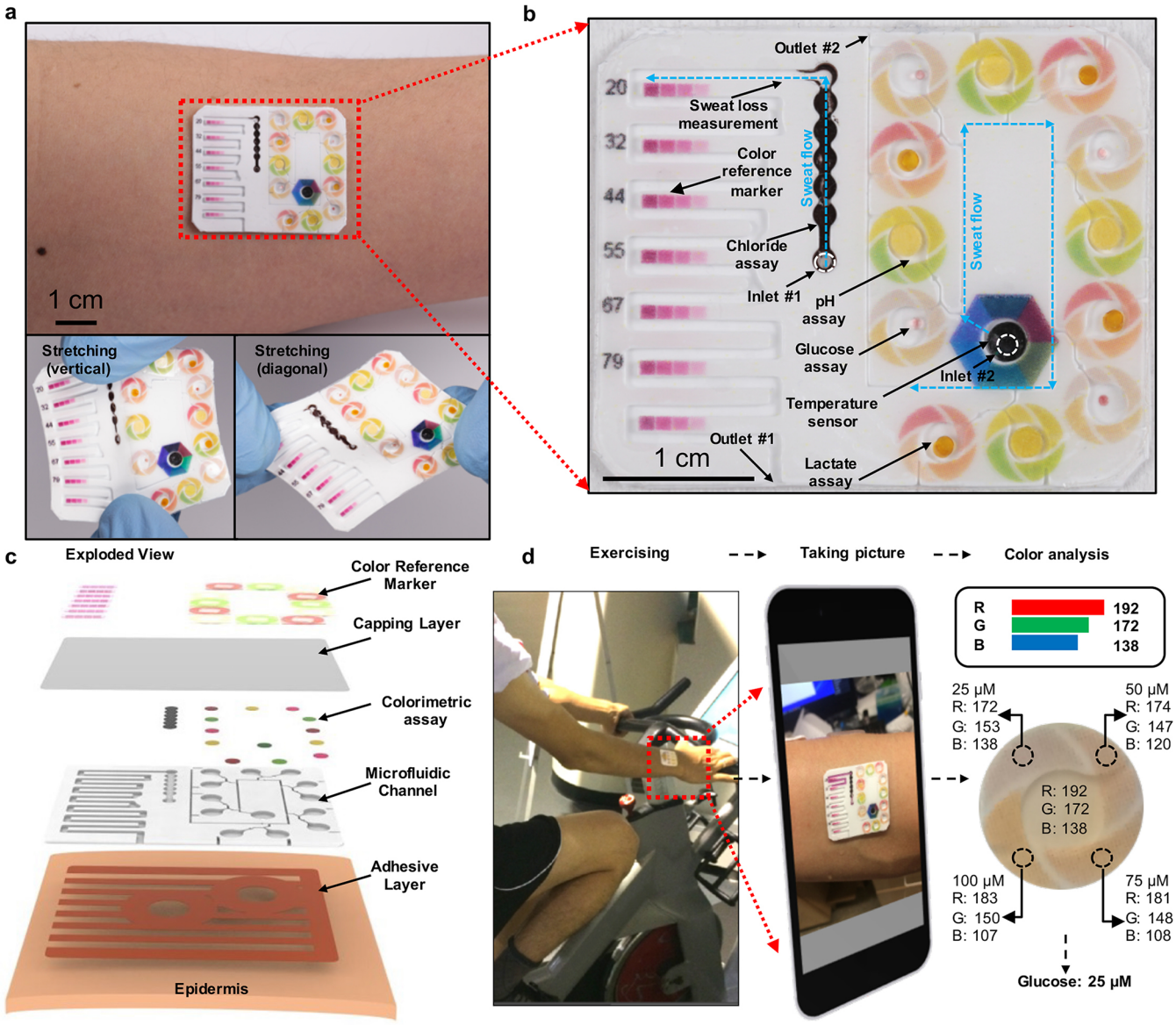

Figure 1. (a) Optical images of soft, flexible microfluidic devices for colorimetric analysis of sweat on the skin (top) and under mechanical deformation with bending (bottom left) and twisting (bottom right). (b) Top view illustration of microfluidic channels filled with blue-dyed water. (c) Exploded view illustration of a device and its interface with the skin. (d) Procedure for collecting sweat samples and color analysis of digital images of the device.

stroke, schizophrenia, diabetes, atopic dermatitis), hydration status, and physical/cognitive fatigue. Mapping variations in the local sweat rate across different body locations provides additional important clues about autonomic thermal regulation and recovery in patients who have suffered a stroke.[1] Similarly, monitoring of sweat rate, electrolyte concentrations, and temperature together can provide important insights into the potential onset of heat exhaustion and heat stroke under extreme environmental conditions.[2] Metabolic alkalosis, in which soft tissues experience elevated pH levels, can be noninvasively characterized by measuring sweat pH.[3] In addition, sweat glucose levels change with diet and exercise, thereby yielding information on prediabetic conditions and athletic performance.[4,5] Similarly, sweat lactate levels correlate with energy metabolism,[6] as an important biomarker for assessing physical fatigue and pressure ischemia.[7] Finally, sodium and chloride concentrations in sweat strongly correlate with dehydration;[8] chloride levels, in particular, are also useful as a screening marker for cystic fibrosis in newborns.[9]

Sweat naturally emerges from pores on the skin where it can be captured using a variety of laboratory techniques for subsequent biomarker analysis. The most common methods rely on absorbent pads taped to the skin for collection, and benchtop capital equipment such as impedance-based spectroscopy and high precision liquid chromatography (HPLC) systems for chemical analysis. Although such approaches yield accurate information, they require expensive, bulky equipment, specialized facilities, and trained personnel; as such, they cannot produce results in real-time or at the point of collection. Recent advances in skin-integrated[10−16] electronic platforms support electrochemical sensors for sweat analysis[17−29] and wireless communication hardware[19,24,30] for data transmission. Systems that exploit near field communication (NFC) or Bluetooth protocols allow data transmission directly to smartphones or other consumer gadgets.[19,24,30] Although these types of sensors

DOI: 10.1021/acssensors.8b01218
ACS Sens. 2019, 4, 379−388

enable continuous monitoring of the concentrations of certain chemical species in sweat, they typically require batteries with other supporting electronics and subsystems that can dominate the form factor and, in certain cases, consequently frustrate seamless, water-tight comfortable interfaces to the skin, particularly during vigorous physical activities. Also, the various calibration procedures needed for operation of most electrochemical sensors limit their use in real-world applications.[27,31]

A recent, separate research direction in this area focuses on thin, soft, skin-compatible microfluidic systems that include networks of microfluidic channels, inlet/outlet ports, microreservoirs, and colorimetric sensors for collection, capture, storage, and analysis of sweat.[32] The attractive cost structures of these systems, together with their simple designs and versatile monitoring capabilities, represent important features that suggest the potential for broad deployment at the point-of-use.[33] Critical to these platforms are the colorimetric chemical assays and associated digital imaging techniques for extracting quantitative information. Previous publications report impressive progress, but with some remaining deficiencies in accurate multianalyte assessments across physiologically relevant ranges of concentrations. For example, in certain previous designs, the continuous flow of sweat through the reaction chambers leads to color leaching, chemical diffusion, and resulting time-dependent, spatially nonuniform color responses that can limit the performance. Also, the reported use of filter paper as a substrate for the assay and as a background for color detection can cause errors associated with uneven color development due to capillary wicking through the paper and concentrating effects at the edges. Furthermore, the prior application of isolated color reference markers at the periphery regions of the device has some utility but cannot eliminate errors in color analysis that arise from spatially uneven lighting conditions. Accurate measurements in practical schemes that are robust against these sources of variability demand additional, advanced design features.

The concepts reported here directly address these needs through functional demonstrations of multifunctional microfluidic platforms for accurate colorimetric analysis of glucose, lactate, pH, chloride, and sweat temperature across a broad range of ambient lighting conditions. Specifically, this work includes (1) integration of multimodal sweat sensing capabilities in a soft, skin-interfaced microfluidic device platform, (2) a collection of optimized capillary bursting valves (CBVs) in the device to direct the flow of sweat to individual microreservoirs for separate assay reactions of multiple assays in single device, without cross-contamination or flow-through mixing effects, (3) color development in the liquid phase, in a manner that provides spatially uniform changes for accurate color measurement, (4) fine-tuned, multiple color reference markers printed directly on the surfaces of these platforms, directly adjacent to each of the microreservoirs, to facilitate real-time quantitative analysis in various lighting conditions, and (5) optimized chemical assays to provide accurate measurements of the concentrations of sweat biomarkers across physiologically relevant ranges. Lab and field studies on simulated sweat and on healthy volunteers yield results that compare favorably with well-established ex situ testing methods.

RESULTS AND DISCUSSION

Soft, Multifunctional Microfluidic Device Designs for Colorimetric Sweat Analysis. Soft microfluidic devices formed in low modulus silicone elastomers by the techniques of soft lithography serve as collection, manipulation, storage, and analysis platforms that are well suited for integration with the skin (Figure 1a). The designs and integrated bioassays reported here support multimodal functionality via lighting-independent colorimetric readout of the concentrations of chloride, glucose, pH, and lactate. Additional related capabilities include measurements of the temperature of sweat and the dynamics of sweat release (rate and total loss). Graphic markings printed on transparent polyester films in colors that precisely match those of the assay reactions laminate onto the top surface of the device to surround each of the microreservoirs and certain segments of the microchannels. These color reference features enable accurate color analysis, largely independent of ambient lighting conditions (Figure 1b). Adding cuts to these polyester overlays yields structures that minimize mechanical constraints on natural deformations of the underlying soft, skin-compatible microfluidic platform (Figure S1). A thermochromic liquid crystal embedded in a separate layer of polyester provides a colorimetric method for determining the temperature of sweat as it emerges from the skin. The resulting platforms avoid mechanically induced irritation at the skin interface, and it facilitates conformal, water-tight seals to the surface of the skin. An enlarged view illustration of the system highlights the various layers (Figure 1c).

The skin adhesion layer that lies between the base of the device and the surface of the skin incorporates openings aligned to two backside inlet ports in the microfluidic system. As sweat leaves the skin pores from these regions, it moves the microfluidic network (serpentine channel and a collection of microreservoirs separated by valves) via pressures associated with action of the eccrine glands, without external pumps, capillarity effects, or actuators.[34] Sweat fills the inlet regions of the device and then perfuses into either a serpentine channel (inlet #1) or a collection of microchannels (inlet #2) that connect to microreservoirs through a series of CBVs. The microreservoirs include thermochromic materials for temperature sensing and chemical or enzymatic reagents for glucose, pH and lactate analysis. The component of the system designed for measurement of sweat rate and total sweat loss also includes a colorimetric chloride assay. This assay, described in detail subsequently, does not require the use of a reservoir with fixed volume, but it does demand a sufficient time for complete reaction, typically 1 min at body temperatures. For this reason, the design for chloride analysis uses a long (1 cm) meandering microchannel to yield uniform color development regardless of sweat rate, even at very high values (Figure S2). The length, together with the cross sectional dimensions and the geometry of the associated inlet, allow for measurements of total sweat loss during a given exercise event, across a wide range of sweat rates and time durations. The other assays use isolated microreservoirs with volumes (5 μL) and depths (600 μm) that yield sufficiently large targets to image easily using smartphone cameras and sufficiently long optical path lengths to produce readily measurable color intensities across physiologically relevant ranges of concentrations for each analyte. Figure 1d shows the process of (1) sweat collection during exercise, (2) image capture using a smartphone camera, and (3) image analysis to determine the temperature of sweat and the concentrations of targeted biomarkers via the use of tailored color reference markers for each assay.

Capillary Bursting Valve Designs for Sequential Sampling of Sweat. A collection of CBVs allows for sequential filling of individual microreservoirs without actuators or moving

DOI: 10.1021/acssensors.8b01218
ACS Sens. 2019, 4, 379−388

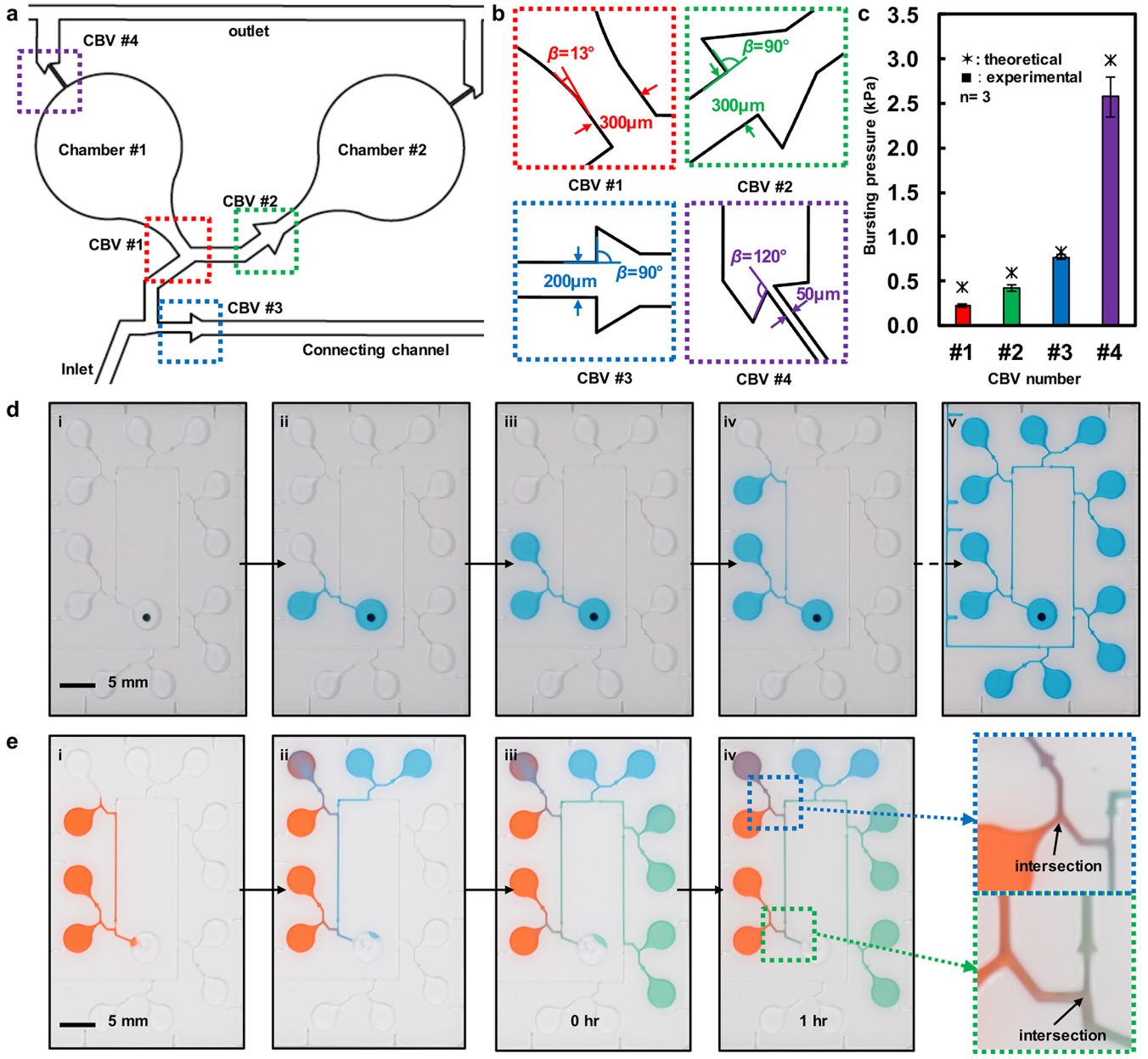

Figure 2. (a) Detailed schematic illustration of a unit cell in a device, including a collection microreservoir, sampling outlet, and four capillary bursting valves (CBV). (b) Sketch of capillary bursting valves with indicated channel width and diverging angle. (c) Experimental results (bars) and theoretical values (asterisk) of capillary bursting values CBV #1, #2, #3, and #4 in the device. (d) Optical images of the working principle of the capillary bursting valves for chrono-sampling. (i) Before entering the collection microreservoir, (ii) filling the collection microreservoir #1, (iii) flowing to microreservoir #2, (iv) flowing to the next microreservoir, and (v) after filling all microreservoirs. (e) Optical images of in vitro testing of chrono-sampling with different colored dyes in water (red, green, and blue) and enlarged images of the interface between different colored dyes.

parts, in a manner that represents an advanced version of schemes outlined in a previous reports.[35] The bursting pressure (BP) of a CBV with a rectangular channel geometry follows from the Young−Laplace equation according to

$$\mathrm{BP} = -2\sigma\left(\frac{\cos\theta_{\mathrm{I}}^{*}}{w} + \frac{\cos\theta_{\mathrm{A}}}{h}\right) \quad (1)$$

where σ is the liquid surface tension, θ_{I}^{*} is the minimum value among $\theta_{\mathrm{A}} + \beta$ and 180° where β is an angle of outlet, θ_{A} is the contact angle of the liquid on channel, and w and h are the width and the height of the channel, respectively. The CBV bursts immediately after the fluidic pressure exceeds the BP; the operation is irreversible. CBVs designed with different BPs allow for passive control over the flow of sweat as it fills into the microchannels. Figure 2a shows a collection of CBVs chronologically labeled (#1−#4), with bursting pressures that increase from #1 to #4. CBV #1 and #2 have similar channel widths (~300 μm) with different outlet angles, 13° and 90°, respectively. By comparison to these CBVs, CBV #3 and #4 have somewhat smaller channel widths (200 and 50 μm) and larger angles (90° and 120°), as shown in Figure 2b. Figure 2c highlights different design parameters that lead to significant differences in BPs for each CBV. Upon entering the microchannels, the filling front approaches the intersection of CBVs #1, #2, and #3 (Figure 1d). The front first bursts through CBV

DOI: 10.1021/acssensors.8b01218
ACS Sens. 2019, 4, 379−388

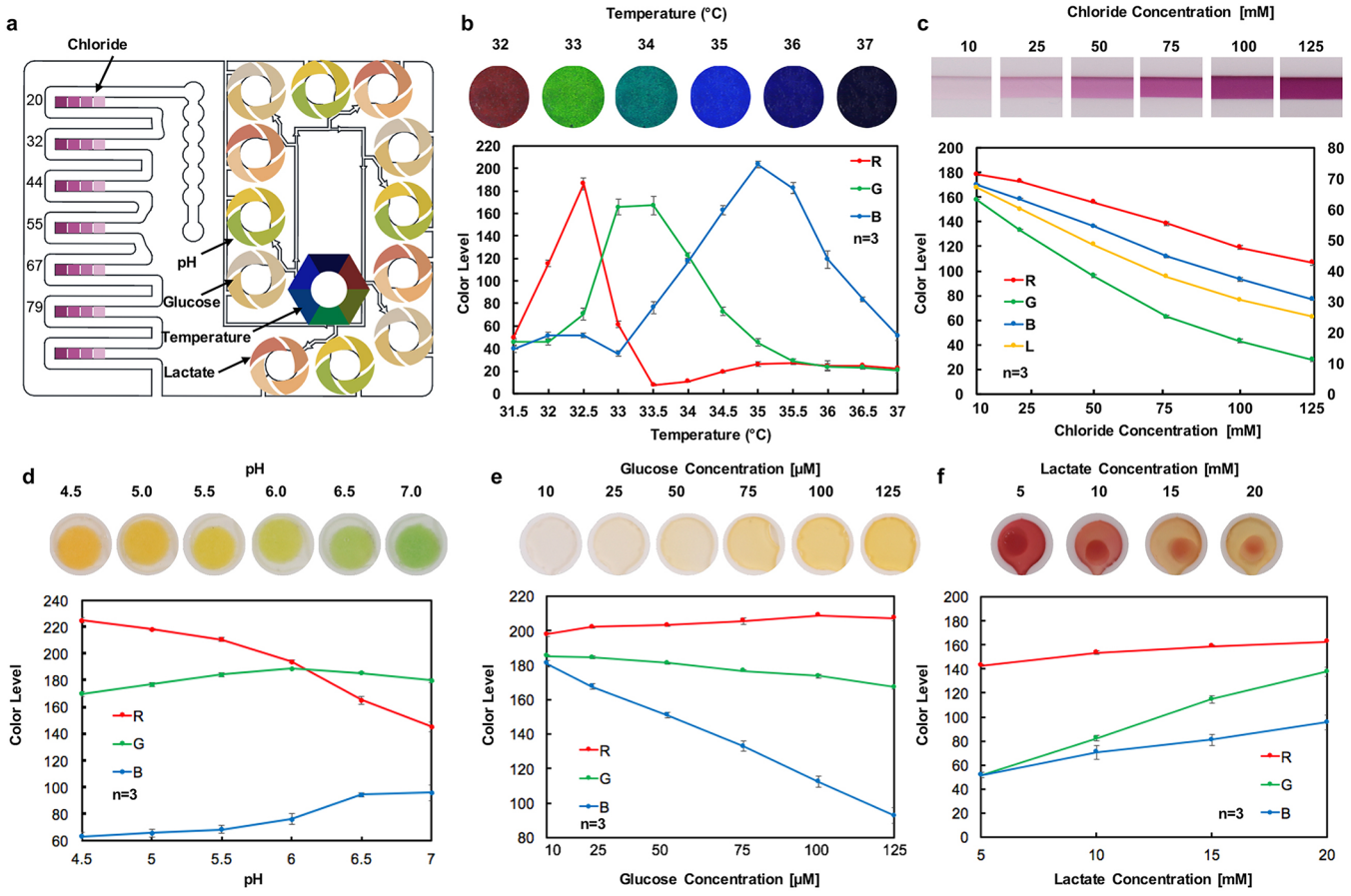

Figure 3. (a) Schematic illustration of a device with color reference markers for chloride, glucose, pH, and lactate analysis and numbers for indicating sweat collection volume. (b) Optical images of the color development of a thermochromic liquid crystal temperature sensor as a function to temperature (top) and color level for each color (bottom). Optical images of color development of assay microreservoirs as a function of sample concentrations (top) and color level for each color (bottom) of (c) chloride, (d) pH, (e) glucose, and (f) lactate.

#1 and starts filling microreservoir #1. Once microreservoir #1 is completely filled, the front bursts into CBV #2, which has the next lowest BP, causing microreservoir #2 to fill. Next, the sweat bursts through CBV #3 and flows into microreservoir #3 through a long channel that provides a damping region to reduce mixing between the reservoirs. Figure 2e illustrates this point, whereby individual microreservoirs sequentially fill with colored fluids without mixing or cross-contamination. The dimensions of the microchannels facilitate laminar flow due to low Reynolds numbers ($\ll$1) over the physiologically relevant range of sweat rates (0−1.0 μL min^{-1}) from collection areas of several square millimeters on the skin.[36] At a sweat rate of ~1 μL min^{-1}, the microreservoirs fill in ~5 min. The flow rate in the microchannels is determined by the sweat rate and the dimensions of the channels and the inlet region. The small intersection area between the microreservoirs (~0.18 mm^2) further minimizes the effects of diffusion. Diffusion-based mixing at the interface of the dyed fluid samples occurs slowly over an extended time period (~1 h) within the small areas of the microchannels that connect adjacent microreservoirs (Figures 2e(iv) and S3). Mechanical deformations from stretching do not induce the cross contamination between the reservoirs or significant errors in measuring sweat volume (Figure S4). These collective features allow for multiple biomarkers to be assessed simultaneously and independently, in real-time, with a single device.

Colorimetric Analysis of Concentration and Graphical Reference Markers. Colorimetric methods for quantitative analysis require color reference markers to enable reliable operation under natural ambient conditions, as a means to compensate for variability in the spectral properties of the illuminating light. Figure 3a highlights markers optimized for colorimetric determination of the temperature of sweat and for analysis of chloride, glucose, pH, and lactate. Digital images collected from a series of in vitro tests with standard samples of simulated sweat define the colors of the printed patterns that form these reference markers. The colorimetric responses of each assay over typical ranges of concentration for each of the targeted chemistries in sweat provide spectral information for the color reference markers.[36,37] A ternary cholesteric liquid crystalline mixture of 40 wt % cholesteryl oleyl carbonate (COC), 40 wt % cholesteryl nonanoate (CN), and 20 wt % cholesteryl 2, 4-dichlorobenzoate (CD) encapsulated by a film of polyester (25 μm thick) with black background serves as a temperature sensor that is red at 32 °C, green at 33 °C, and blue at 34 °C, thereby enabling colorimetric determination of temperature across a range from 31 to 37 °C (Figures 3b and S5).

The chloride assay uses silver chloranilate immobilized in polyhydroxyethyl methacrylate (pHEMA). Here, purple colored ions result from reactions with chloride ions in sweat.[38] The porous hydrogel structure of pHEMA immobilizes opaque white precipitates of AgCl that form from the reaction, thereby

DOI: 10.1021/acssensors.8b01218
ACS Sens. 2019, 4, 379−388

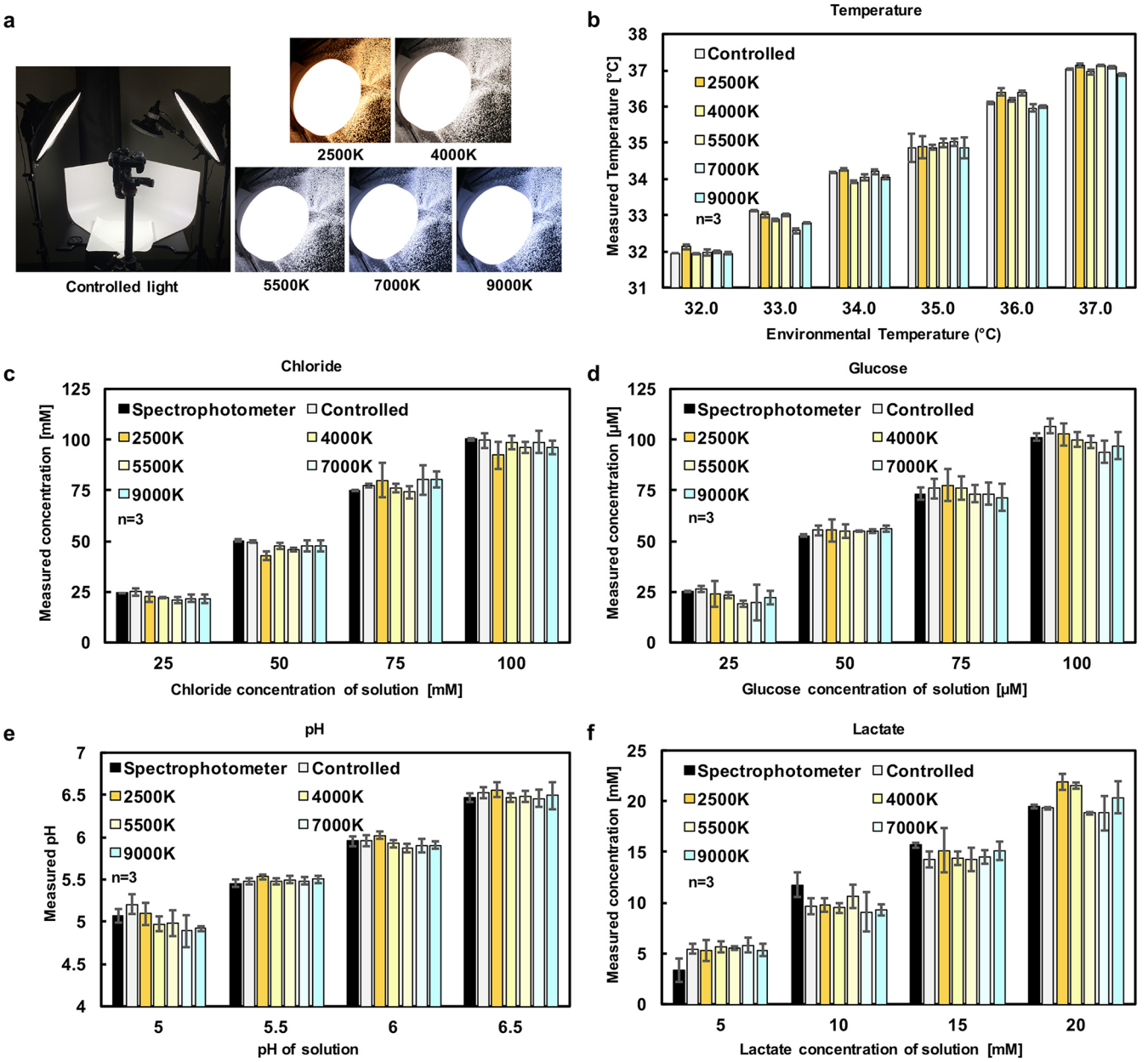

Figure 4. (a) Pictures of in vitro tests of color reference markers in various light sources of controlled light, with five different color temperatures of light. (b) Measured temperature using color reference markers on the device at different environmental temperatures in various lighting conditions. Measured concentration using a spectrophotometer and color reference markers on the device filled with standard solutions of (c) chloride, (d) glucose, (e) pH, and (f) lactate with various lighting conditions.

eliminating their effect on color extraction. The result is a significant reduction in the RGB color levels (dark purple color) with an increase in chloride ion concentration. Here, the lightness (L) level from Lab color space provides a representative number to define the color intensity of the assay (Figure 3c).[39] As shown in Figure 3d, the pH assay is a commercial indicator that turns increasingly green with increasing pH, thereby decreasing the depth of red color in the assay paper.

By contrast to chemical reactions and analytics described for temperature, chloride, and pH, the glucose assay requires multiple stages and produces hydrogen peroxide (H_2O_2) as a byproduct of an enzymatic reaction with glucose oxidase. H_2O_2 reacts with glucose substrate dye, resulting in a yellowish color whose intensity corresponds to the concentration of glucose in sweat (Figure 3e). For physiologically relevant values, the pH and the lactate concentration do not affect the response of the glucose assay (Figure S6).

As with glucose, the lactate assay relies on enzymatic reactions, but which yield a red color at low concentrations (~5 mM) and yellow at high concentrations (~15 mM). Here, the green level changes monotonically across this range, thereby serving as a good choice of measurement parameter for this assay (Figure 3f). For physiologically relevant values, the pH and the glucose concentration do not affect to the response of the lactate assay (Figure S7). Changing the pH from 5.5 to 6.5 causes an apparent change in lactate concentration of ~2 mM. The pH determined from the pH sensor can, however, be used to calibrate for this effect. The glucose and lactate assays respond only to glucose and lactate, respectively (Figures S6 and S7).

DOI: 10.1021/acssensors.8b01218
ACS Sens. 2019, 4, 379−388

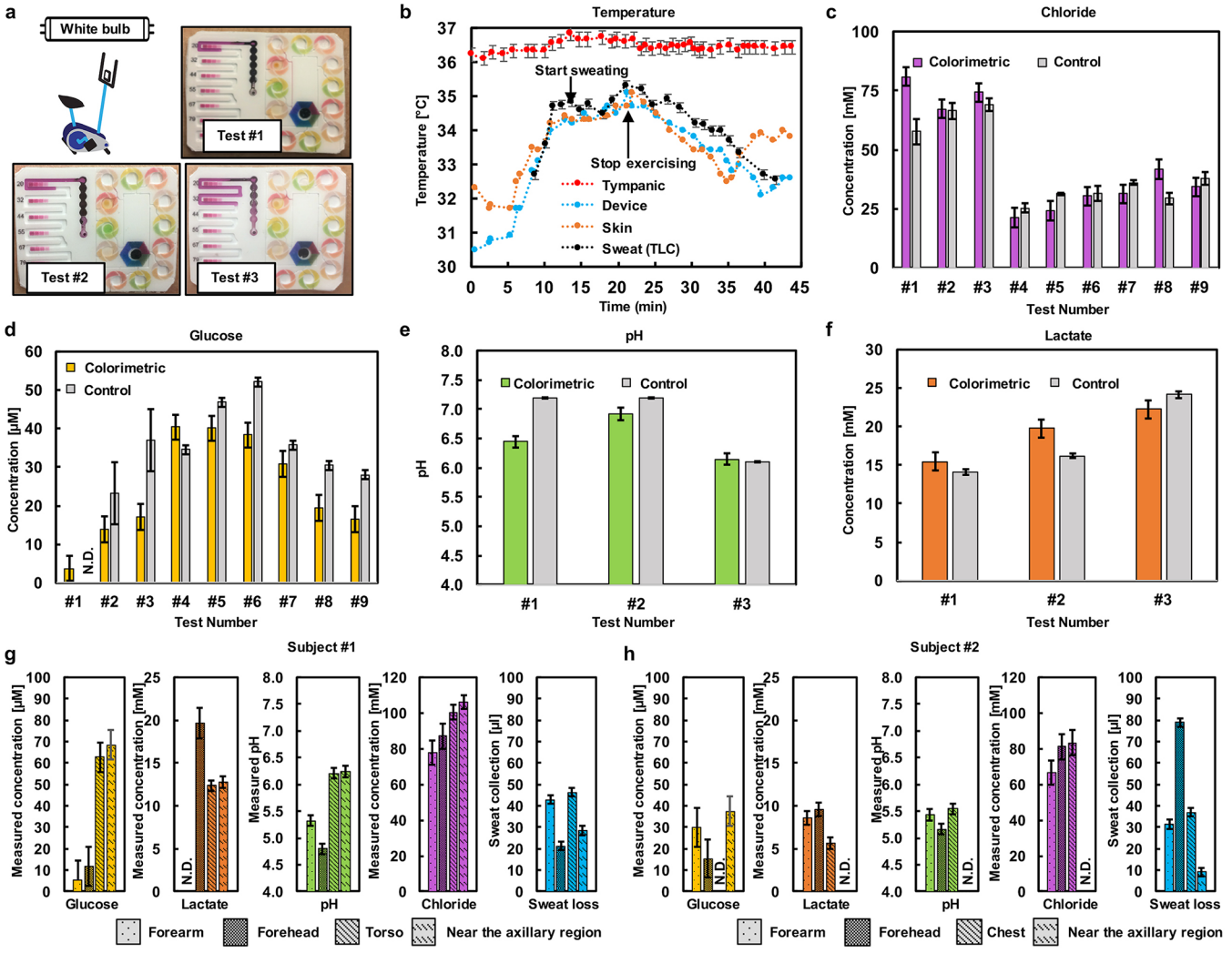

Figure 5. (a) Optical images of microfluidic devices after use in three in situ trials. (b) Measured temperature of sweat using TLC temperature sensor, and of the tympanic, device, and skin regions using an infrared thermometer. Sweat (c) chloride, (d) glucose, (e) pH, and (f) lactate concentration from colorimetric methods and control tests from three in situ trials. N.D. represents data not collected due to concentrations below the detection range. Regional variations of sweat concentration (glucose, lactate, pH, chloride, and sweat loss) from different body positions; forearm, forehead, chest, and below the armpit from subject (g) #1 and (h) #2. N.D. represents data not collected due to insufficient sweat generation.

While the sensors for temperature, chloride and pH provide reversible operation, enzymatic assays are not reversible. The pH and chloride assays develops color quickly (<1 and <3 min, respectively); the enzymatic assays require ∼15 min for full color development (Figures S2 and S8). The shelf life of each of the chemical assays for chloride, pH, glucose and lactate assays is longer than 20 days under storage conditions of 20 °C and 40% relative humidity (Figure S9).

In all cases, the depth of the microreservoir defines the path length for optical absorption (Figure S10). Increasing the depth enhances the color change. The choice of 600 μm balances this consideration with the need to maintain a low bending stiffness and a low profile form factor for effective integration with the skin. The geometries yield volumes of sweat (∼5 μL) that are relevant for performance monitoring during physical exertion. The reservoirs remove the effects of flow rate on the color development of the glucose, lactate and pH assays. The final selections of color reference markers correspond to colors that capture temperature (32, 33, 34, 35, 36, 37 °C), chloride (25, 50, 75, 100 mM), glucose (25, 50, 75, 100 μM), pH (5.0, 5.5, 6.0, 6.5), and lactate (5, 10, 15, 20 mM) over physiologically relevant ranges (Figure S11). The color reference markers reside on the top polyester layer, in patterns that completely encircle each microreservior, to enable accurate color measurement across a wide range of lighting conditions.

Accuracy Testing of Colorimetric Analysis under Various Lighting Conditions. The absolute colors extracted from digital images of the colorimetric assays depend on ambient lighting conditions and associated color temperatures: 2500 K (sunrise, sunset), 4000 K (neutral white), 5500 K (daylight), 7000 K (cloudy day), and 9000 K (shade under a blue sky). These conditions, however, affect the colorimetric assays and color reference markers in a similar manner. Systematic studies demonstrate that proper use of these markers can yield accurate and reliable extraction of color information for color temperatures between 2500 and 9000 K, as well as in yellow light, white light, and sunlight (Figure 4a). Spectroscopic measurements of each assay, prepared separately in microtubes, define the upper limits on the accuracy that can be obtained with these chemistries (Figure 4b−f, Table S1). The uncertainties associated with this method are ∼1 mM for chloride, ∼3 μM for glucose, ∼0.1 for pH, and ∼2 mM for lactate. The limited

DOI: 10.1021/acssensors.8b01218
ACS Sens. 2019, 4, 379−388

accuracy for lactate follows from a 1 mM value of K_m (Michaelis−Menten constant) for LOx and from its saturated response (Figure S12). Measurements based on digital imaging under controlled lighting yield uncertainties of ∼0.2 °C in temperature and other results that are only slightly worse than those obtained by spectroscopic analysis: ∼ 2 mM for chloride, ∼7 μM for glucose, and ∼0.1 for pH. The uncertainties for lactate are ∼1 mM, somewhat better than those via spectroscopy, mainly because the color reference marker in this case does not depend on linear correlation but instead uses the actual colors at each concentration for comparison.

For variable lighting conditions and use of color reference markers, the uncertainties are ∼0.2 °C for temperature, ∼7 mM for chloride, ∼8 μM for glucose, ∼0.1 for pH, and ∼2 mM for lactate (Figures 4b−f and S13, Table S1). Sources of these uncertainties include inconsistent color development in the chemical assay (present in all evaluation approaches), insufficient intensities for light with low color temperature, and insufficiently robust colors in the reference markers. (Tables S1 and S2). The accuracy of the colorimetric measurement can be increased by increasing the range of color change over the target concentrations or pH values or temperatures. Contamination of the top side of the device by dust, debris, lotions, or other substances has the potential to lead to errors in color extraction. Use of a commercial color reference chart (ColorChecker Passport Photo, X-Rite, Inc.) eliminates this third source of uncertainty.[40] For chloride analysis, a photoediting program helps to define reference color levels for each chloride concentration (Figure S14a). Images captured with ambient lighting can be modified using the ColorChecker to yield accuracy results similar to those obtained under controlled lighting conditions (Figure S14b−d).

In Situ Colorimetric Analysis of Sweat in Field Studies. Field testing with healthy volunteers during cycling exercises under white bulb lighting conditions illustrates the performance in scenarios of practical interest (Figure 5a). Temperature analysis of sweat based on devices attached to the side of the forehead yields values of 32.7 ± 0.1 °C after 8 min of exercising, with gradual increases to 35.3 ± 0.1 °C, comparable to findings from previous studies,[41] until the end of the cycling, after which the temperature decreases continually to the rest state (Figure 5b). Use of an infrared camera yields similar results (Figures 5b, S15, and S16). The surface temperature in regions away from the device show larger spatial fluctuations than those of the device due to variabilities in evaporation rate from uneven sweating (Figure S17). The device eliminates the effect of evaporative cooling and renders an improved estimate of body temperature. The temperature of the dermis, where the sweat glands are located, is 1−2 °C hotter than that of the epidermis.[42] Nevertheless, the low flow rates of sweat (∼1 μL/min) lead to thermal equilibration of sweat temperature with the epidermis.

Measurements of concentrations of chloride in sweat determined from devices mounted on the forearm are between 21 and 81 mM across nine trials. These values are within the normal range (Figures 5c and S8),[43] and all results, except for those associated with test #1, are consistent with those obtained using a chloridometer for analysis of sweat collected by a coil-shaped PDMS microfluidic device placed next to the colorimetric device, where the difference is ∼23 mM. We associate these differences with local skin contamination or bilateral variations. The fundamental limitation of this comparison is that the collecting regions are different for the colorimetric and conventional methods, which could lead to differences in concentrations.[44]

The concentration of glucose in sweat determined from devices mounted on the forearm across nine trials falls between 4 and 40.4 μM. These values, which are approximately 100× smaller than normal blood glucose levels, are in a range consistent with that of previous studies (Figures 5d and S19).[17,18,45,46] The control measurements for tests #1−#3 rely on analysis by nuclear magnetic resonance (NMR), where the largest discrepancies are ∼24 μM (test #2 and #3). The disadvantage of NMR is that it requires a relatively large amount of sweat (1 mL), outside of the range that can be captured easily using the microfluidic platforms described here. As an alternative, spectroscopic analysis of the same colorimetric assay in the device yield differences that are smaller than 14 μM. Sweat pH levels measured with the sweat microfluidics devices ranged between 6.1 and 6.9, in good agreement with previous studies (Figure 5e).[47] Sweat lactate concentrations lie between 15 to 22 mM. These results are comparable to the values reported in previous research and to those determined using the conventional method (Figure 5f).[48]

Figure 5g and h shows results from the forearm, forehead, torso, and near the axillary region in two subjects (Figure S20). The experiments involve deployment of devices on regions of the body with different curvatures and shapes. Subject #1 shows higher concentrations of glucose, lactate, and chloride compared to subject #2. Glucose levels in subject #1 vary across different body locations, whereas subject #2 shows little variation with body location. Measurements from the torso region yield higher chloride levels than the peripheral regions, consistent with previous findings.[36,49] Lactate levels are greater at the forehead region compared to the chest, also consistent with previous findings.[44] Sweat pH does not vary significantly as a function of body position in these subjects. In contrast, the rate and local loss of sweat vary considerably with position. Sweat loss in subject #1 is lowest at the forehead, whereas the forehead region is a source of heavy sweat loss in subject #2. Additional tests show strong correlations between local sweat loss and total body loss (Figure S21).

CONCLUSION

The soft, skin-compatible, multimodal microfluidic devices introduced in this study represent powerful platforms for the capture, storage, and colorimetric analysis of sweat biomarkers, rate, loss and temperature. Integrated color reference markers provide accurate colorimetric estimates of analyte concentrations under various lighting conditions and in remote settings. Field trials in healthy subjects demonstrate these capabilities in ambulatory modes of use with accuracies matching those of conventional methods. Taken together, these results establish the multifunctional capabilities of skin-mounted microfluidic systems for sweat analysis, with bioassays relevant to monitoring hydration and managing health disorders. Certain applications, especially those that involve physical contact (such as football), may demand improvements in the mechanical robustness of the soft microfluidic structure, without sacrificing favorable characteristics of the skin interface. Another direction of possible interest is in the integration of electronic physiological sensor modules to expand the functionality to include biophysical measurements.

DOI: 10.1021/acssensors.8b01218
ACS Sens. 2019, 4, 379−388

■ ASSOCIATED CONTENT

Supporting Information

The Supporting Information is available free of charge on the ACS Publications website at DOI: 10.1021/acssensors.8b01218.

Details on the fabrication process, color analysis, and body test results (PDF)

■ AUTHOR INFORMATION

Corresponding Author

*E-mail: jrogers@northwestern.edu.

ORCID

Jungil Choi: 0000-0002-3659-8978

Jonathan T. Reeder: 0000-0002-7624-7355

John A. Rogers: 0000-0002-2980-3961

Author Contributions

J.C. and A.J.B contributed equally to this study. J.C., A.J.B, and J.A.R. conceived the project, designed the studies, analyzed and interpreted the data. J.C. developed microfluidics, glucose, chloride assay, temperature sensors, and color reference marker. A.J.B. developed the pH and lactate sensors. J.T.R., T.R.R., A.T., S.B.K., N.N., A.H.-F., J.B.M., and A.J.A. assisted in device fabrication. S.X. provided physiological advises. J.C. and A.J.B. conducted the experiments. J.C., A.J.B., R.G., and J.A.R. wrote the manuscript.

Notes

The authors declare no competing financial interest.

■ ACKNOWLEDGMENTS

This work utilized Northwestern University Micro/Nano Fabrication Facility (NUFAB), which is partially supported by Soft and Hybrid Nanotechnology Experimental (SHyNE) Resource (NSF ECCS-1542205), the Materials Research Science and Engineering Center (DMR-1720139), the State of Illinois, and Northwestern University. We thank the Center for Bio-Integrated Electronics for support of this work.

■ REFERENCES

(1) Korpelainen, J. T.; Sotaniemi, K. A.; Myllyla, V. V. Hyperhidrosis as a Reflection of Autonomic Failure in Patients with Acute Hemispheral Brain Infarction - an Evaporimetric Study. *Stroke* **1992**, *23* (9), 1271−1275.

(2) Epstein, Y.; Roberts, W. O. The pathopysiology of heat stroke: an integrative view of the final common pathway. *Scand J. Med. Sci. Spor* **2011**, *21* (6), 742−748.

(3) Patterson, M. J.; Galloway, S. D. R.; Nimmo, M. A. Effect of induced metabolic alkalosis on sweat composition in men. *Acta Physiol. Scand.* **2002**, *174* (1), 41−46.

(4) Moyer, J.; Wilson, D.; Finkelshtein, I.; Wong, B.; Potts, R. Correlation Between Sweat Glucose and Blood Glucose in Subjects with Diabetes. *Diabetes Technol. Ther.* **2012**, *14* (5), 398−402.

(5) Hawley, J. A.; Leckey, J. J. Carbohydrate Dependence During Prolonged, Intense Endurance Exercise. *Sports Med.* **2015**, *45*, S5−S12.

(6) Pilardeau, P.; Vaysse, J.; Garnier, M.; Joublin, M.; Valeri, L. Secretion of eccrine sweat glands during exercise. *Br. J. Sports Med.* **1979**, *13* (3), 118−21.

(7) Polliack, A.; Taylor, R.; Bader, D. Sweat analysis following pressure ischaemia in a group of debilitated subjects. *J. Rehabil. Res. Dev* **1997**, *34* (3), 303−8.

(8) Morgan, R. M.; Patterson, M. J.; Nimmo, M. A. Acute effects of dehydration on sweat composition in men during prolonged exercise in the heat. *Acta Physiol. Scand.* **2004**, *182* (1), 37−43.

(9) Farrell, P. M.; Rosenstein, B. J.; White, T. B.; Accurso, F. J.; Castellani, C.; Cutting, G. R.; Durie, P. R.; LeGrys, V. A.; Massie, J.; Parad, R. B.; Rock, M. J.; Campbell, P. W. Guidelines for diagnosis of cystic fibrosis in newborns through older adults: Cystic Fibrosis Foundation consensus report. *J. Pediatr.* **2008**, *153* (2), S4−S14.

(10) Kim, D. H.; Lu, N.; Ma, R.; Kim, Y. S.; Kim, R. H.; Wang, S.; Wu, J.; Won, S. M.; Tao, H.; Islam, A.; Yu, K. J.; Kim, T. I.; Chowdhury, R.; Ying, M.; Xu, L.; Li, M.; Chung, H. J.; Keum, H.; McCormick, M.; Liu, P.; Zhang, Y. W.; Omenetto, F. G.; Huang, Y.; Coleman, T.; Rogers, J. A. Epidermal electronics. *Science* **2011**, *333* (6044), 838−43.

(11) Webb, R. C.; Bonifas, A. P.; Behnaz, A.; Zhang, Y.; Yu, K. J.; Cheng, H.; Shi, M.; Bian, Z.; Liu, Z.; Kim, Y. S.; Yeo, W. H.; Park, J. S.; Song, J.; Li, Y.; Huang, Y.; Gorbach, A. M.; Rogers, J. A. Ultrathin conformal devices for precise and continuous thermal characterization of human skin. *Nat. Mater.* **2013**, *12* (10), 938−44.

(12) Han, S.; Kim, J.; Won, S. M.; Ma, Y.; Kang, D.; Xie, Z.; Lee, K. T.; Chung, H. U.; Banks, A.; Min, S.; Heo, S. Y.; Davies, C. R.; Lee, J. W.; Lee, C. H.; Kim, B. H.; Li, K.; Zhou, Y.; Wei, C.; Feng, X.; Huang, Y.; Rogers, J. A. Battery-free, wireless sensors for full-body pressure and temperature mapping. *Sci. Transl. Med.* **2018**, *10* (435), No. eaan4950.

(13) Zhu, C. X.; Chortos, A.; Wang, Y.; Pfattner, R.; Lei, T.; Hinckley, A. C.; Pochorovski, I.; Yan, X. Z.; To, J. W. F.; Oh, J. Y.; Tok, J. B. H.; Bao, Z. A.; Murmann, B. Stretchable temperature-sensing circuits with strain suppression based on carbon nanotube transistors. *Nature Electronics* **2018**, *1* (3), 183−190.

(14) Xu, B. X.; Akhtar, A.; Liu, Y. H.; Chen, H.; Yeo, W. H.; Park, S. I. I.; Boyce, B.; Kim, H.; Yu, J. W.; Lai, H. Y.; Jung, S. Y.; Zhou, Y. H.; Kim, J.; Cho, S.; Huang, Y. G.; Bretl, T.; Rogers, J. A. An Epidermal Stimulation and Sensing Platform for Sensorimotor Prosthetic Control, Management of Lower Back Exertion, and Electrical Muscle Activation. *Adv. Mater.* **2016**, *28* (22), 4462−4471.

(15) Yamada, T.; Hayamizu, Y.; Yamamoto, Y.; Yomogida, Y.; Izadi-Najafabadi, A.; Futaba, D. N.; Hata, K. A stretchable carbon nanotube strain sensor for human-motion detection. *Nat. Nanotechnol.* **2011**, *6* (5), 296−301.

(16) Webb, R. C.; Ma, Y.; Krishnan, S.; Li, Y.; Yoon, S.; Guo, X.; Feng, X.; Shi, Y.; Seidel, M.; Cho, N. H.; Kurniawan, J.; Ahad, J.; Sheth, N.; Kim, J.; Taylor, J. G., VI; Darlington, T.; Chang, K.; Huang, W.; Ayers, J.; Gruebele, A.; Pielak, R. M.; Slepian, M. J.; Huang, Y.; Gorbach, A. M.; Rogers, J. A. Epidermal devices for noninvasive, precise, and continuous mapping of macrovascular and microvascular blood flow. *Sci. Adv.* **2015**, *1* (9), No. e1500701.

(17) Lee, H.; Choi, T. K.; Lee, Y. B.; Cho, H. R.; Ghaffari, R.; Wang, L.; Choi, H. J.; Chung, T. D.; Lu, N.; Hyeon, T.; Choi, S. H.; Kim, D. H. A graphene-based electrochemical device with thermoresponsive microneedles for diabetes monitoring and therapy. *Nat. Nanotechnol.* **2016**, *11* (6), 566−572.

(18) Lee, H.; Song, C.; Hong, Y. S.; Kim, M. S.; Cho, H. R.; Kang, T.; Shin, K.; Choi, S. H.; Hyeon, T.; Kim, D. H. Wearable/disposable sweat-based glucose monitoring device with multistage transdermal drug delivery module. *Sci. Adv.* **2017**, *3* (3), No. e1601314.

(19) Gao, W.; Emaminejad, S.; Nyein, H. Y.; Challa, S.; Chen, K.; Peck, A.; Fahad, H. M.; Ota, H.; Shiraki, H.; Kiriya, D.; Lien, D. H.; Brooks, G. A.; Davis, R. W.; Javey, A. Fully integrated wearable sensor arrays for multiplexed in situ perspiration analysis. *Nature* **2016**, *529* (7587), 509−514.

(20) Cho, E.; Mohammadifar, M.; Choi, S. A Single-Use, Self-Powered, Paper-Based Sensor Patch for Detection of Exercise-Induced Hypoglycemia. *Micromachines* **2017**, *8* (9), 265.

(21) Abellan-Llobregat, A.; Jeerapan, I.; Bandodkar, A.; Vidal, L.; Canals, A.; Wang, J.; Morallon, E. A stretchable and screen-printed electrochemical sensor for glucose determination in human perspiration. *Biosens. Bioelectron.* **2017**, *91* (C), 885−891.

(22) Jia, W.; Bandodkar, A. J.; Valdes-Ramirez, G.; Windmiller, J. R.; Yang, Z.; Ramirez, J.; Chan, G.; Wang, J. Electrochemical tattoo biosensors for real-time noninvasive lactate monitoring in human perspiration. *Anal. Chem.* **2013**, *85* (14), 6553−60.

(23) Imani, S.; Bandodkar, A. J.; Mohan, A. M.; Kumar, R.; Yu, S.; Wang, J.; Mercier, P. P. A wearable chemical-electrophysiological

DOI: 10.1021/acssensors.8b01218
ACS Sens. 2019, 4, 379−388

hybrid biosensing system for real-time health and fitness monitoring. *Nat. Commun.* **2016**, *7*, 11650.
(24) Rose, D. P.; Ratterman, M. E.; Griffin, D. K.; Hou, L.; Kelley-Loughnane, N.; Naik, R. R.; Hagen, J. A.; Papautsky, I.; Heikenfeld, J. C. Adhesive RFID Sensor Patch for Monitoring of Sweat Electrolytes. *IEEE Trans. Biomed. Eng.* **2015**, *62* (6), 1457−65.
(25) Emaminejad, S.; Gao, W.; Wu, E.; Davies, Z. A.; Nyein, H. Y. Y.; Challa, S.; Ryan, S. P.; Fahad, H. M.; Chen, K.; Shahpar, Z.; Talebi, S.; Milla, C.; Javey, A.; Davis, R. W. Autonomous sweat extraction and analysis applied to cystic fibrosis and glucose monitoring using a fully integrated wearable platform. *Proc. Natl. Acad. Sci. U. S. A.* **2017**, *114* (18), 4625−4630.
(26) Glennon, T.; O'Quigley, C.; McCaul, M.; Matzeu, G.; Beirne, S.; Wallace, G. G.; Stroiescu, F.; O'Mahoney, N.; White, P.; Diamond, D. 'SWEATCH': A Wearable Platform for Harvesting and Analysing Sweat Sodium Content. *Electroanalysis* **2016**, *28* (6), 1283−1289.
(27) Bandodkar, A. J.; Molinnus, D.; Mirza, O.; Guinovart, T.; Windmiller, J. R.; Valdes-Ramirez, G.; Andrade, F. J.; Schoning, M. J.; Wang, J. Epidermal tattoo potentiometric sodium sensors with wireless signal transduction for continuous non-invasive sweat monitoring. *Biosens. Bioelectron.* **2014**, *54* (C), 603−9.
(28) Nyein, H. Y. Y.; Gao, W.; Shahpar, Z.; Emaminejad, S.; Challa, S.; Chen, K.; Fahad, H. M.; Tai, L. C.; Ota, H.; Davis, R. W.; Javey, A. A Wearable Electrochemical Platform for Noninvasive Simultaneous Monitoring of Ca2+ and pH. *ACS Nano* **2016**, *10* (7), 7216−7224.
(29) Bandodkar, A. J.; Hung, V. W.; Jia, W.; Valdes-Ramirez, G.; Windmiller, J. R.; Martinez, A. G.; Ramirez, J.; Chan, G.; Kerman, K.; Wang, J. Tattoo-based potentiometric ion-selective sensors for epidermal pH monitoring. *Analyst* **2013**, *138* (1), 123−8.
(30) Kim, J.; Jeerapan, I.; Imani, S.; Cho, T. N.; Bandodkar, A.; Cinti, S.; Mercier, P. P.; Wang, J. Noninvasive Alcohol Monitoring Using a Wearable Tattoo-Based Iontophoretic-Biosensing System. *Acs Sensors* **2016**, *1* (8), 1011−1019.
(31) Guinovart, T.; Bandodkar, A. J.; Windmiller, J. R.; Andrade, F. J.; Wang, J. A potentiometric tattoo sensor for monitoring ammonium in sweat. *Analyst* **2013**, *138* (22), 7031−8.
(32) Choi, J.; Ghaffari, R.; Baker, L. B.; Rogers, J. A. Skin-interfaced systems for sweat collection and analytics. *Sci. Adv.* **2018**, *4* (2), No. eaar3921.
(33) Koh, A.; Kang, D.; Xue, Y.; Lee, S.; Pielak, R. M.; Kim, J.; Hwang, T.; Min, S.; Banks, A.; Bastien, P.; Manco, M. C.; Wang, L.; Ammann, K. R.; Jang, K. I.; Won, P.; Han, S.; Ghaffari, R.; Paik, U.; Slepian, M. J.; Balooch, G.; Huang, Y.; Rogers, J. A. A soft, wearable microfluidic device for the capture, storage, and colorimetric sensing of sweat. *Sci. Transl. Med.* **2016**, *8* (366), 366ra165.
(34) Choi, J.; Xue, Y. G.; Xia, W.; Ray, T. R.; Reeder, J. T.; Bandodkar, A. J.; Kang, D.; Xu, S.; Huang, Y. G.; Rogers, J. A. Soft, skin-mounted microfluidic systems for measuring secretory fluidic pressures generated at the surface of the skin by eccrine sweat glands. *Lab Chip* **2017**, *17* (15), 2572−2580.
(35) Choi, J.; Kang, D.; Han, S.; Kim, S. B.; Rogers, J. A. Thin, Soft, Skin-Mounted Microfluidic Networks with Capillary Bursting Valves for Chrono-Sampling of Sweat. *Adv. Healthcare Mater.* **2017**, *6* (5), 1601355.
(36) Sonner, Z.; Wilder, E.; Heikenfeld, J.; Kasting, G.; Beyette, F.; Swaile, D.; Sherman, F.; Joyce, J.; Hagen, J.; Kelley-Loughnane, N.; Naik, R. The microfluidics of the eccrine sweat gland, including biomarker partitioning, transport, and biosensing implications. *Biomicrofluidics* **2015**, *9* (3), 031301.
(37) Bariya, M.; Nyein, H. Y. Y.; Javey, A. Wearable sweat sensors. *Nature Electronics* **2018**, *1* (3), 160.
(38) Barney, J.; Bertolacini, R. Colorimetric determination of chloride with mercuric chloranilate. *Anal. Chem.* **1957**, *29* (8), 1187−1188.
(39) Araki, H.; Kim, J.; Zhang, S. N.; Banks, A.; Crawford, K. E.; Sheng, X.; Gutruf, P.; Shi, Y. Z.; Pielak, R. M.; Rogers, J. A. Materials and Device Designs for an Epidermal UV Colorimetric Dosimeter with Near Field Communication Capabilities. *Adv. Funct. Mater.* **2017**, *27* (2), 1604465.
(40) Linero, O.; Cidad, M.; Arana, G.; Nguyen, C.; de Diego, A. The use of a standard digital camera as an inexpensive, portable, fast and non-destructive analytical tool to measure colour: Estimation of the ripening stage of tomatoes (Solanum lycopersicum) as a case study. *Microchem. J.* **2017**, *134*, 284−288.
(41) Nadel, E. R.; Bullard, R. W.; Stolwijk, J. A. Importance of skin temperature in the regulation of sweating. *J. Appl. Physiol.* **1971**, *31* (1), 80−87.
(42) Saxena, V. P. Temperature distribution in human skin and subdermal tissues. *J. Theor. Biol.* **1983**, *102* (2), 277−86.
(43) Shirreffs, S. M.; Maughan, R. J. Whole body sweat collection in humans: An improved method with preliminary data on electrolyte content. *J. Appl. Physiol.* **1997**, *82* (1), 336−341.
(44) Patterson, M. J.; Galloway, S. D.; Nimmo, M. A. Variations in regional sweat composition in normal human males. *Exp Physiol* **2000**, *85* (6), 869−75.
(45) Moyer, J.; Wilson, D.; Finkelshtein, I.; Wong, B.; Potts, R. Correlation between sweat glucose and blood glucose in subjects with diabetes. *Diabetes Technol. Ther.* **2012**, *14* (5), 398−402.
(46) Chen, Y.; Lu, S.; Zhang, S.; Li, Y.; Qu, Z.; Chen, Y.; Lu, B.; Wang, X.; Feng, X. Skin-like biosensor system via electrochemical channels for noninvasive blood glucose monitoring. *Sci. Adv.* **2017**, *3* (12), No. e1701629.
(47) Oncescu, V.; O'Dell, D.; Erickson, D. Smartphone based health accessory for colorimetric detection of biomarkers in sweat and saliva. *Lab Chip* **2013**, *13* (16), 3232−8.
(48) Green, J. M.; Bishop, P. A.; Muir, I. H.; McLester, J. R., Jr.; Heath, H. E. Effects of high and low blood lactate concentrations on sweat lactate response. *Int. J. Sports Med.* **2000**, *21* (8), 556−60.
(49) Taylor, N. A.; Machado-Moreira, C. A. Regional variations in transepidermal water loss, eccrine sweat gland density, sweat secretion rates and electrolyte composition in resting and exercising humans. *Extrem Physiol Med.* **2013**, *2* (4), 4.

DOI: 10.1021/acssensors.8b01218
ACS Sens. 2019, 4, 379−388